No.	K25-2173	
Project Title	Establishing pre-clinical models to study functions of intellectual disability associated caused by a variant in the synaptotagmin 4 (SYT4) gene	
Principal Investigator	Natini Jinawath (Faculty of Medicine Ramathibodi Hospital, Mahidol University・Associate professor)	
Project Member(s)	IMSUT Host Researcher	Yoichi Furukawa (The Institute OF Medical Science, The University Of Tokyo・Professor)
	Project Member (s)	Natini Jinawath (Division of Translational Medicine, Chakri Naruebodindra Medical Institute, Faculty of Medicine Ramathibodi Hospital, Mahidol University・Associate Professor)
	Project Member (s)	Nithi Asavapanumas (Pre-clinic, Chakri Naruebodindra Medical Institute, Faculty of Medicine Ramathibodi Hospital, Mahidol University・Senior Lecturer)
	Project Member (s)	Nilubon Singhto (Ramathibodi Comprehensive Cancer Center, Faculty of Medicine Ramathibodi Hospital, Mahidol University・Researcher)
	Project Member (s)	Yoichi Furukawa (Division of Clinical Genome Research・Professor)
	Project Member (s)	Kiyoshi Yamaguchi (Division of Clinical Genome Research・Associate Professor)
	Project Member (s)	Seiya Imoto (Human Genome Center・Professor)
	Project Member (s)	Meiko Takahashi (Center for Genomic Medicine, Kyoto University, Graduate School of Medicine・Senior Lecturer)

(Form 2)

Principal Investigator
Natini Jinawath, MD, PhD

IMSUT International Joint Usage/Research Center Project <International>

Joint Research Report (Annual/Project Completion)

Annual Report

Report

1. **Research title:** Establishing pre-clinical models to study functions of intellectual disability associated caused by a variant in the synaptotagmin 4 (SYT4) gene

2. Background and rationales

Non-syndromic global developmental delay (NS-GDD) is characterized by the inability to accomplish developmental milestones within the expected age range [AlMutiri, R et al, *Children (Basel)* 2023]. This implies a substantial delay in two or more developmental domains in children aged five years or less. Developmental domains comprise gross and fine motor skills, speech and language, cognition, personal-social skills, and activities of daily living. Intellectual disability (ID) includes impairments in general cognitive capacities that impact both intellectual functioning, including learning and thinking, and adaptive functioning, which pertains to everyday living tasks such as communication and daily living [AlMutiri, R et al]. The global prevalence of NS-GDD presented up to 1-3% in children aged 5 years or younger [Banerjee, S et al, *Front Genet* 2022]. The prevalence of ID is 2.7% in children and 2.17% in adults, respectively [Banerjee, S et al]. The causes of NS-GDD/ID can be derived from heterogeneity factors, including the genetic and acquired factors [Aldosari, AN, *Clin Exp Pediatr* 2024]. While the precise etiology is frequently unresolved, genetic factors account for approximately fifty percent of all cases [Aldosari, AN]. We examined the family tree with exhibiting NS-GDD/ID throughout four generations at the genetic counseling clinic of the Faculty of Medicine, Ramathibodi Hospital. The results of whole-exome sequencing (WES) revealed that a single nucleotide variation (SNV) in the synaptotagmin 4 (SYT4) gene had been identified in the affected family members (**Figure 1**).

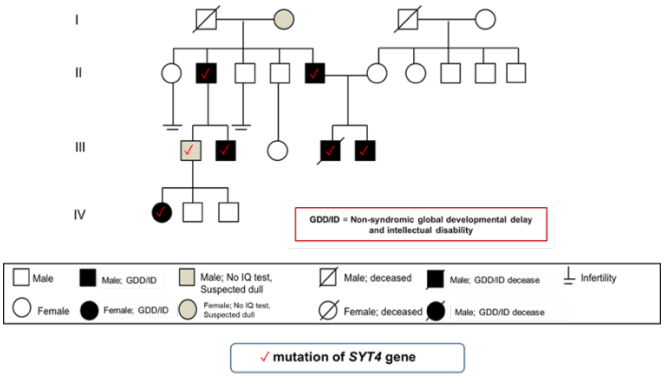

Figure 1: Pedigree of family members affected by NS-GDD/ID

This missense variant in *SYT4* results in the substitution of alanine at position 169 with threonine (p. Ala169Thr), suggesting that the is likely to be pathogenic and associated with NS-GDD/ID in this family. Nevertheless, the effects of the *SYT4* mutation underlying NS-GDD/ID remain unclear. For an experimental design, we performed the gene editing (knock-in) using CRISPR-Cas technology in induced human pluripotent stem cells (iPSCs), and subsequently induce the differentiation of the iPSCs into neuron cells. We performed scRNA-seq on both wild-type and mutant iPSC-derived neurons to characterize neuronal subtype differentiation, maturation, functional properties, and neurodegeneration-related pathways. Our first-year findings demonstrated that SYT4 mutation disrupts neuronal lineage specification, maturation, and metabolic homeostasis while inducing maladaptive inflammatory and neurodegeneration-related pathways. Homozygous *SYT4* mutants showed the most severe abnormalities. In the second year, we will validate these effects using independent clones, integrate transcriptomic and proteomic analyses, and perform functional assays to determine how SYT4 loss alters synaptic activity, stress responses, and neuronal physiology. Ultimately, this research aims to elucidate SYT4-mediated disease mechanisms and support the development of prognostic, diagnostic, and therapeutic strategies for NS-GDD/ID.

3. Objectives

3.1 To differentiate the *SYT4* mutant iPSCs to neural cells and perform single-cell transcriptomic analysis

3.2 To examine the cellular proteome in both sets (set1 and set2) for confirmation of the transcriptome results

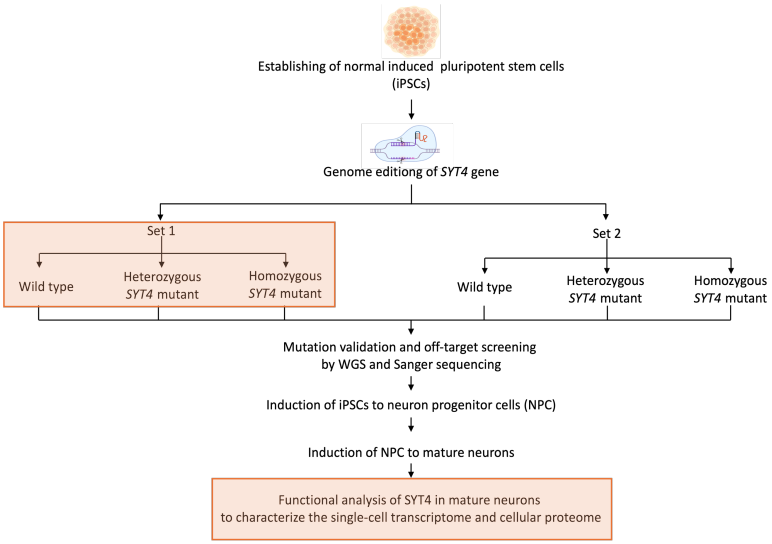

☐ = The experiment is the collaborative part with IMSUT, the University of Tokyo.

Figure 2: Schematic workflow of an experimental design

4. Work plans for the entire project

Experiments	Year 1 2025 (FY2025 joint research grant)				Year 2 2026 (FY2026 joint research grant)				Year 3 2027			
	1-3	4-6	7-9	10-12	1-3	4-6	7-9	10-12	1-3	4-6	7-9	10-12
Induction of iPSCs into mature neuronal cells in set 1	✓	✓	✓									
cDNA library preparation from iPSCs derived neuron cells in set1 for single-cell RNA sequencing			✓									
• Characterization of mature neuronal cells in set 1 using scRNA-seq • scRNA-seq data analysis and comparison of *SYT4* variant frequencies *Collaborative part with IMSUT				✓								
Sample preparation for secretome and cellular proteome analysis by LC-MS/MS (3 biological replicates)				X	X							
Induction of iPSCs into mature neuronal cells in set 2					X	X						
cDNA library preparation from iPSCs derived neuron cells in set 2 for single-cell RNA sequencing							X					
• Characterization of mature neuronal cells in set 2 using scRNA-seq (at IMSUT) • scRNA-seq data analysis of mature neuronal cells in set 2 • Integration of scRNA-seq and bulk proteomics								⊗	⊗			
Spatial omics analysis of the brain organoids derived from wild type and *SYT4* mutant samples									X	X		
Functional analysis validation e.g., oxidative stress, inflammatory response, calcium imaging, electrophysiology, and synaptic function assays				X	X	X	X	X	X	X	X	

Note. ✓= The experiment has already been done.,
X = The experiment is an ongoing process in sample preparation.
⊗ = The experiment is the collaborative part with IMSUT, the University of Tokyo

5. Project's progress since adopted (For Year 1: FY2025 joint research grant)

5.1 Whole genome sequencing

In this experiment, a single-stranded oligodeoxynucleotide (ssODN) repair template containing the desired *SYT4* point mutation was co-delivered with the Cas9-sgRNA plasmid into human iPSCs. This genome-editing strategy successfully generated three isogenic iPSC lines representing wild-type, heterozygous *SYT4* mutant, and homozygous *SYT4* mutant genotypes (**Figure 3A**). The mutation status of each clone was verified by whole-genome sequencing (**Figure 3B**), which confirmed the precise nucleotide substitution at chr18:g.40853889C>T and validated the establishment of the three edited iPSC genotypes. These validated iPSC clones were subsequently differentiated into neurons for downstream SYT4 functional and molecular analyses.

A

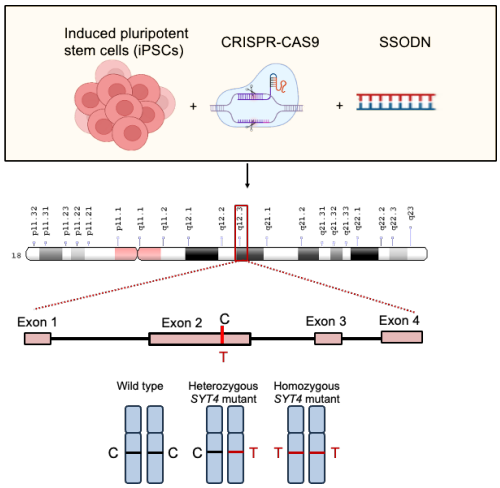

B

Figure 3: (**A**) Schematic workflow of *SYT4* genome-editing generated three isogenic human iPSC and (**B**) whole genome sequencing results

5.2 iPSC-derived neuron differentiation and mature neuron gene marker validation

Differentiation of human iPSCs into neuronal lineages was accompanied by clear morphological maturation and an increase in the expression of neuronal markers. Phase-contrast imaging showed that undifferentiated iPSCs initially formed compact, iPSC-like colonies (**Figure 4A**). After 8 days of neural induction, these iPSC colonies presented an epithelial-like morphology characteristic of neural progenitor cells (NPCs), with cells displaying a more elongated shape and organized, sheet-like arrangement (**Figure 4A**). By day 14 of differentiation, the NPCs further matured into neurons, exhibiting a neurite-bearing morphology with extensive processes and complex cellular networks(**Figure 4A**). To confirm neuronal differentiation at the molecular level, we assessed the expression of mature neuronal marker genes, including microtubule-associated protein 2 (*MAP*2), beta-III-tubulin (*TUBB3*), synaptotagmin 4 (*SYT4*), glial fibrillary acidic protein (*GFAP*), glutamate decarboxylase 67 (*GAD67),* and vesicular glutamate transporter 1 (*VGLUT1*), by RT-qPCR, comparing neurons with NPCs for each genotype. Across all genotypes, neurons showed higher expression of neuronal markers relative to NPCs (**Figure 4B**). These results suggested that we successfully induced the iPSCs into neuron cells.

A

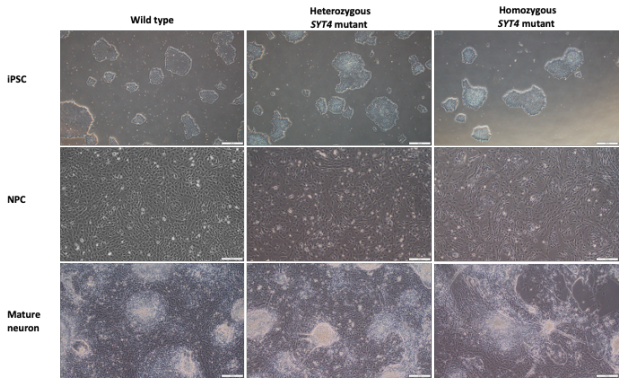

B

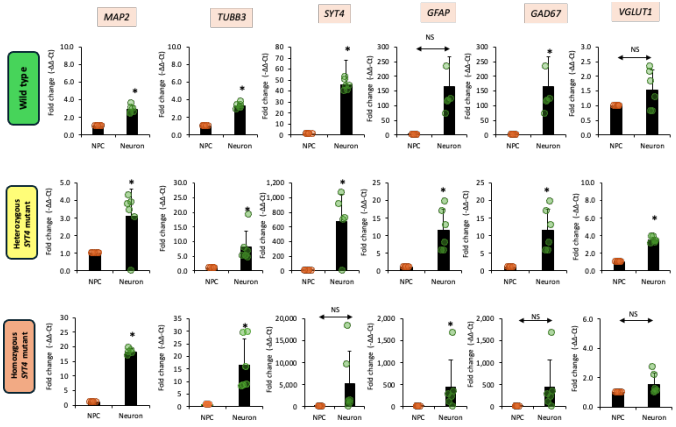

Figure 4: Morphological maturation changes and neuronal marker expression in a human iPSC-derived neurons. (**A**) Representative phase-contrast images illustrating the transition from iPSC-like colonies (upper row) to epithelial-like neural progenitor cells (NPCs; middle row) after 8 days of differentiation, followed by the acquisition of neurite-bearing neuronal morphology at the mature neuron stage after 14 days of differentiation (lower row). (**B**) RT–qPCR analysis of mature neuronal marker genes in neurons compared with NPCs for each genotype. Bars graph represent mean ± SD of six measurements from three biological replicates. Statistical significance was assessed using unpaired student's *t*-test, with $P < 0.05$ considered significant. * = statistical significance, NS= non-significance

5.3 Characterization of cellular heterogeneity of human iPSC-derived neuron using scRNA-seq

To assess the cellular heterogeneity and cellular population subtypes of *SYT4* mutations during neuronal differentiation, we performed single-cell RNA sequencing (scRNA-seq) on a human iPSC-derived neuronal cell generated from wild type (WT), heterozygous SYT4-mutant (Het_D1), and homozygous SYT4-mutant (Homo_F5) lines. We firstly perform a QC assessment to demonstrate the improvements after filtering low-quality cells. Prior to filtering, the three genotypes showed broad variation in the number of detected genes (nFeature_RNA), UMI counts (nCount_RNA), and mitochondrial transcript percentages (percent.mt) (**Figure 5A, left panel**). After applying standard QC thresholds (nFeature_RNA = 2500-900, nCount_RNA = 35,000, and percent.mt < 5), the retained cells displayed comparable nFeature_RNA and nCount_RNA distributions with markedly reduced mitochondrial percentages across all genotypes (**Figure 5A, right panel**), supporting the inclusion of high-quality cells for downstream analysis.

To characterize the neuron cell population, we examined the expression of neuronal stem cell, neuron progenitor cell, and neuronal maturation markers across UMAP data (**Figure 5B**). Pluripotent and early neural markers (*SOX2, PAX6, NES*) were enriched in progenitor-like cell clusters, whereas neuronal lineage markers (*DCX, TUBB3, MAP2, NEUROD1, ASCL1*) localized to differentiation and maturation neuronal clusters. For neuronal subtype specific markers, GAD1 (inhibitory neurons), TH (dopaminergic lineage), and *SLC17A6* (glutamatergic neurons), were distinctly expressed in subtype-specific regions of the UMAP. Glial markers (*GFAP, S100B*) and oligodendrocyte-related genes (*OLIG2, MBP*) identified smaller populations of non-neuronal cells.

From the aforementioned gene markers, cell clustering and cell-type annotation revealed nine major cell populations, including neural progenitor cells, proliferating NPCs, intermediate progenitors, transitioning inhibitory neurons, inhibitory neurons, transitioning glutamatergic neurons, mature glutamatergic neurons, astrocytes, and fibroblasts (**Figure 5C**).

A

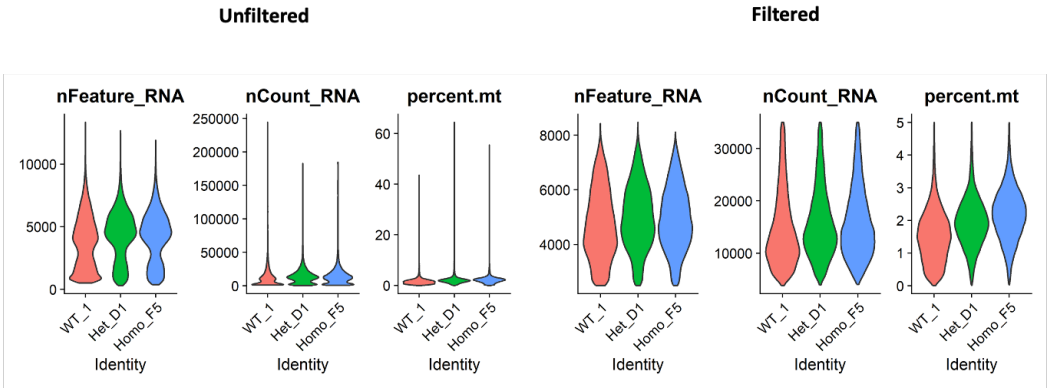

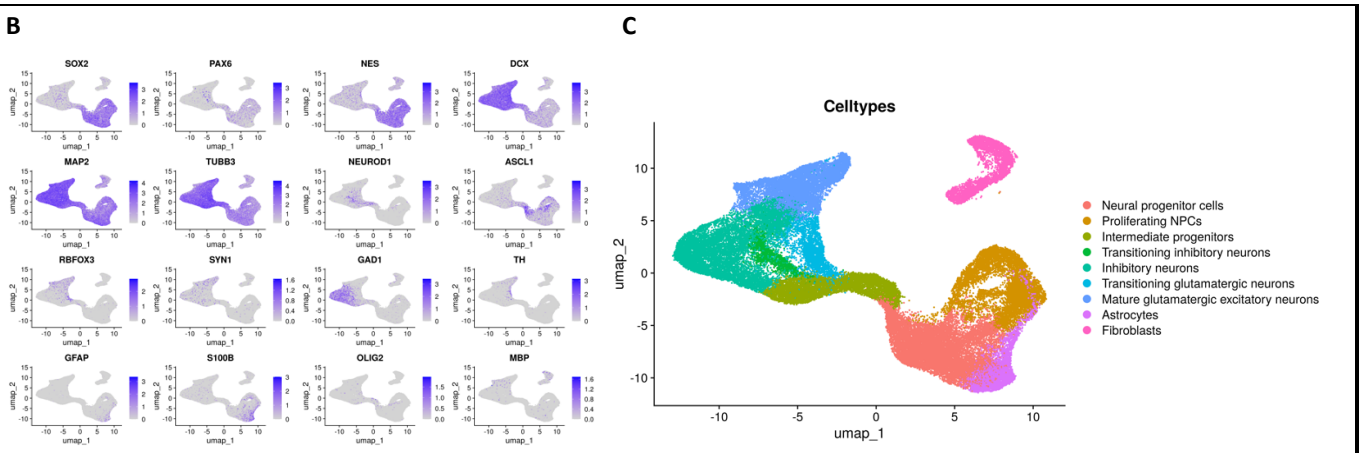

Figure 5: Data filtering, cell-type annotation and cell population clustering in iPSC-derived neurons. (**A)** Violin plots summarizing single-cell RNA-seq quality control metrics for iPSC-derived neurons from wild-type (WT_1), heterozygous *SYT4*-mutant (Het_D1), and homozygous *SYT4*-mutant (Homo_F5) lines. For each sample, the distributions of detected genes per cell (nFeature_RNA), total UMI counts per cell (nCount_RNA), and the percentage of mitochondrial transcripts (percent.mt) are shown before (left) and after (right) quality filtering, with each violin representing all cells from one line. **(B)** UMAP plots showing the marker genes expression for the major neuron population subtype. (**C)** UMAP plots showing the marker genes expression for the neuron population subtypes.

5.4 Trajectory and pseudotime analysis of neuronal lineage

To examine the neuronal lineage after *SYT4* mutation, this study further performed trajectory and pseudotime analyses to determine whether *SYT4* mutation alters neuron differentiation. For trajectory analysis, most populations were present across all genotypes, indicating that the *SYT4* mutation does not abolish the ability of iPSCs to generate diverse neural lineages under differentiation conditions (**Figure 6A**). All three genotypes contributed cells to each major cluster, although subtle shifts in cluster density and distribution were apparent (**Figure 6A**). However, we observed that the inhibitory neuron and astrocyte were rarely observed in the homozygous *SYT4* mutant condition. In addition, intermediate progenitor neurons were dramatically reduced in cell density in the heterozygous *SYT4* mutant condition (**Figure 6A**). These patterns suggested that the SYT4 variant might disrupt lineage specification and might influence the proportion or maturation trajectory of specific neuronal populations. Trajectory analysis revealed that *SYT4* mutation alters neuronal differentiation in a dosage-dependent manner, with heterozygous cells showing dysregulated and premature developmental progression, while homozygous mutant cells exhibit a stronger block in terminal neuronal maturation and relative accumulation of immature neuronal states (**Figure 6B**). Pseudotime analysis demonstrated a conserved overall developmental path from stem/progenitor to mature neuronal states across all genotypes, but *SYT4*-mutant condition showed an alteration of module dynamics. Heterozygous cells displayed earlier loss of stem/progenitor programs and transiently enhanced maturation signatures, whereas homozygous mutant cells showed a more dramatically enrichment of immature neuronal signatures with comparatively delayed and less coordinated acquisition of mature neuronal features, consistent with impaired neuronal maturation (**Figure 6C**).

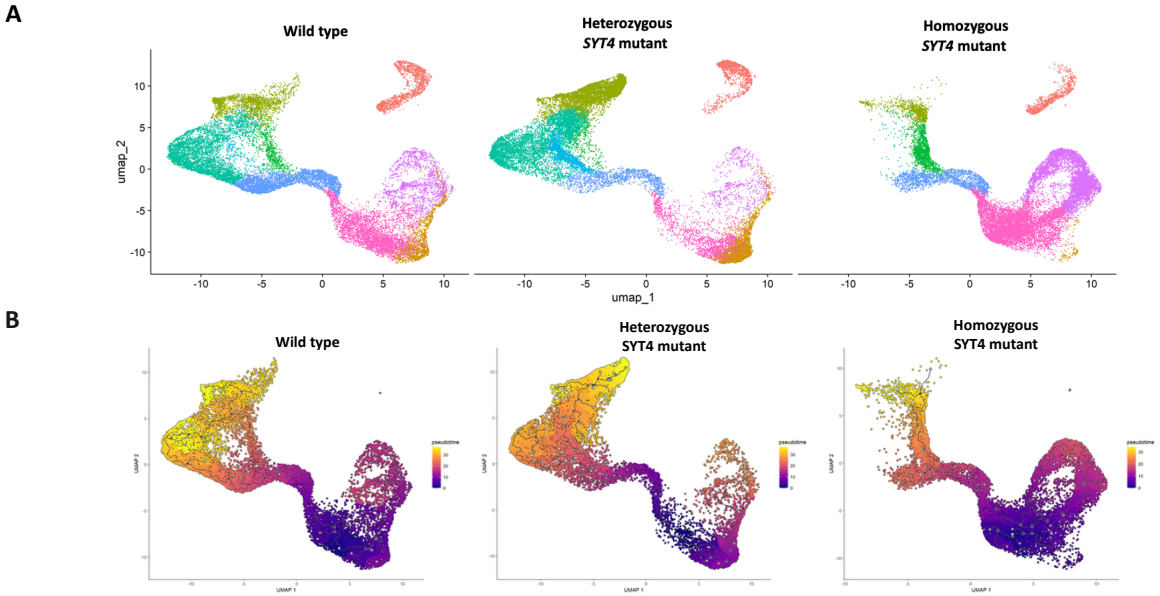

C

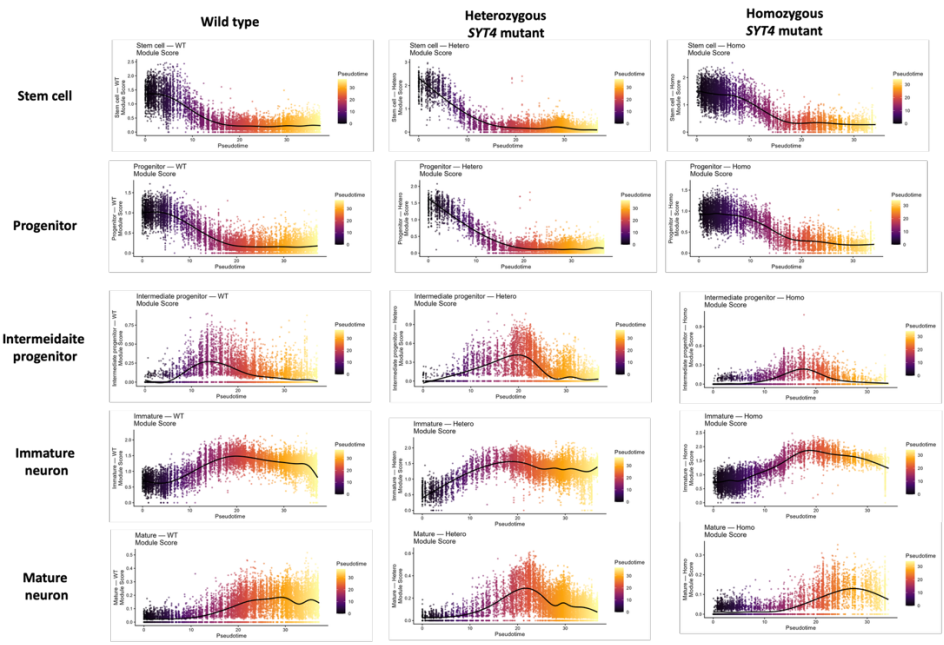

Figure 6: Single cell trajectory and pseudotime analysis of a human iPSC-derived neuron cell after *SYT4* mutant. (A) UMAP visualization showing that cells derived from wild type, heterozygous *SYT4* mutant, and homozygous *SYT4* mutant lines form distinct, partially overlapping clusters, reflecting both shared and genotype specific transcriptional state. UMAP visualization colored by cell type population clusters **(B)** UMAP of learned trajectory analysis from cell type clustering with cells ordered in pseudotime. Dark purple represents early developmental stages (root) and yellow indicating terminal differentiated states. **(C)** Scatter plots with smoothing line showing the module scores for gene markers in each neuron subtype (stem cell, progenitor, intermediate progenitor, immature neuron and mature neuron) for WT (left column), heterozygous *SYT4* mutant (middle column), and homozygous *SYT4* mutant (right column). Each dot represents a single-cell and the color represents the pseudotime, which the dark purple represents early developmental stages (root) and yellow indicating terminal differentiated states.

5.4 Enriched gene ontology (GO) terms for differentially expressed gene (DEG) of each cell population subtype

In this section, we examined Gene Ontology (GO) terms enriched from differentially expressed genes (DEGs) identified in the cell populations of interest across each group.

5.4.1 Astrocyte: GO enrichment analysis comparing wild-type and heterozygous *SYT4* mutants revealed that down-regulated genes were strongly enriched in neurodevelopmental and synaptic regulatory pathways, including synapse assembly, postsynaptic organization, axon guidance, neuron projection development, and cognition-associated processes (**Figure 7A, left panel**). These changes suggested a diminished capacity for astrocyte-mediated support of neuronal maturation and synaptic function. In contrast, up-regulated genes in heterozygous *SYT4* mutants were enriched in pathways related to cell-cycle regulation and chromosomal segregation, such as mitotic sister chromatid separation, nuclear division, chromosome segregation, and spindle organization, indicating an increasing activation of proliferative and mitotic programs (**Figure 7A, right panel**). Collectively, these findings indicated that partial loss of *SYT4* disrupts astrocytic homeostasis by attenuating neuro-supportive pathways while enhancing cell-cycle–related activity.

5.4.2 Inhibitory neuron: A similar analysis was performed for inhibitory neurons. Comparison between wild-type and heterozygous *SYT4* mutants demonstrated that down-regulated genes were significantly enriched in pathways involved in inhibitory synaptic signaling, neuronal excitability, and higher-order cognitive and circuit-level processes (**Figure 7B, left panel**). Up-regulated DEGs in heterozygous mutants were predominantly associated with extracellular matrix (ECM) remodeling, tissue structural organization, developmental and morphogenetic pathways, and cell-cycle–related functions (**Figure 7B, right panel**). These results suggest that inhibitory neurons in heterozygous *SYT4* mutants exhibit functional decline in synaptic transmission and inhibitory neurotransmission while concomitantly activating programs related to ECM restructuring, tissue morphogenesis, and non-neuronal developmental processes.

5.4.3 Excitatory neuron: GO enrichment analysis of DEGs in excitatory neurons revealed a genotype-dependent disruption of synaptic and neurodevelopmental pathways associated with *SYT4* deficiency. In the wild-type versus heterozygous comparison, down-regulated genes were enriched in synaptic processes related to neurotransmission and learning, including synaptic vesicle exocytosis, neurotransmitter transport, and postsynaptic assembly, suggesting early impairments in excitatory synaptic function (**Figure 7C, left-upper panel**).Up-regulated pathways were linked to Wnt signaling, axon guidance, and cytoskeletal remodeling, suggesting the presence of compensatory structural responses following partial *SYT4* loss (**Figure 7C, left-upper panel**).

In the comparison between wild-type and homozygous mutants, *SYT4*-null excitatory neurons showed increased expression in pathways associated with neuronal maturation, developmental morphogenesis, and synaptic specialization(**Figure 7C, right-upper panel**) , while simultaneously exhibiting obvious down-regulation of ribosome biogenesis, ribonucleoprotein complex assembly, cytoplasmic translation, RNA splicing, and mitochondrial gene expression and organization (**Figure 7C, right-upper panel**). This opposing pattern suggested that, in the absence of functional SYT4, neurons may attempt to transcriptionally activate maturation and synapse related programs as a compensatory mechanism. However, the concurrent reduction in biosynthetic and mitochondrial pathways indicates that these neurons lack the metabolic and translational capacity necessary to execute these maturation programs at the functional level. A similar expression pattern was observed when comparing heterozygous and homozygous *SYT4* mutants, reinforcing the interpretation that loss of *SYT4* initiates an incomplete compensatory response aimed at restoring synaptic development (**Figure 7C, lower panel**). Nevertheless, protein-level validation will be required to confirm whether these transcriptomic alterations translate into functional deficits in excitatory neuronal maturation and synaptic activity.

A

Astrocyte

Wild type VS Heterozygous *SYT4* mutant

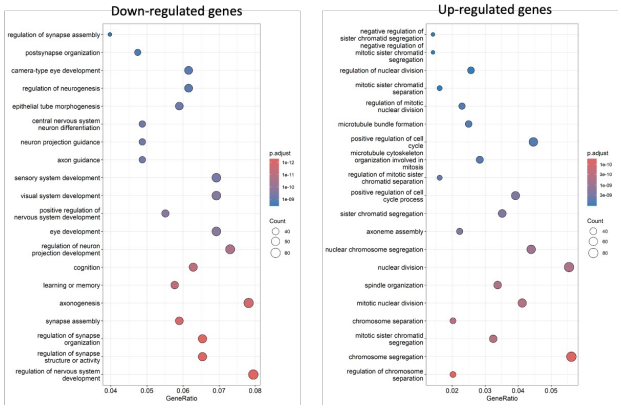

B

Inhibitory neuron

Wild type VS Heterozygous *SYT4* mutant

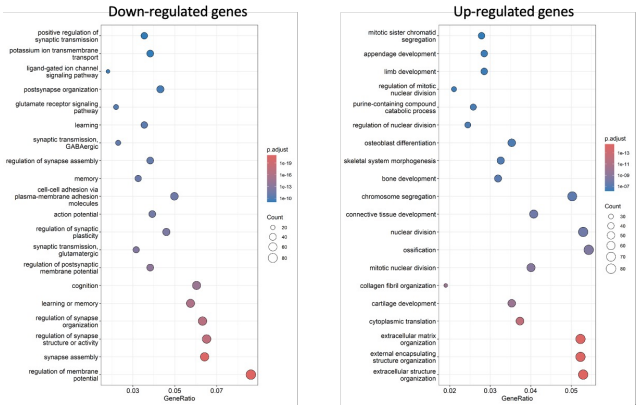

C

Excitatory neuron

Wild type VS Heterozygous *SYT4* mutant

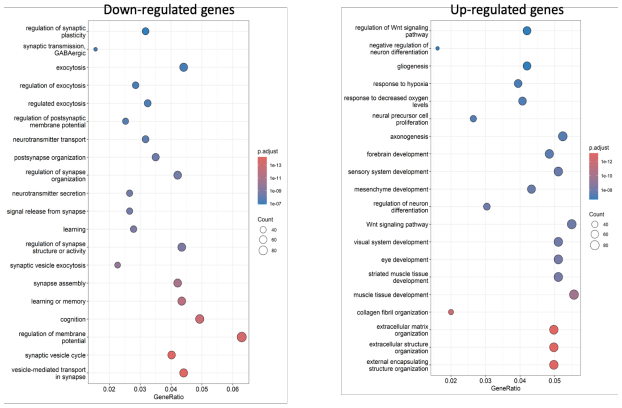

Wild type VS Homozygous *SYT4* mutant

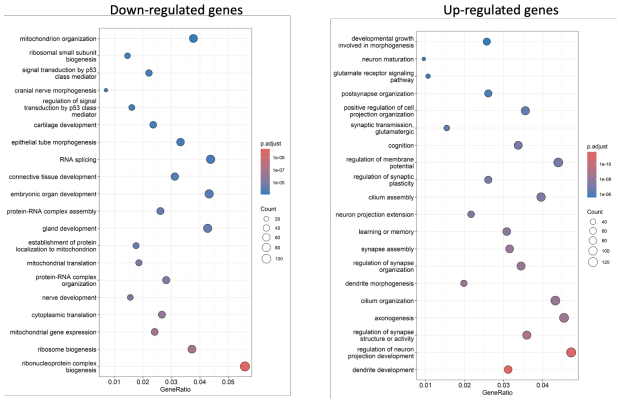

Heterozygous *SYT4* mutant VS Homozygous *SYT4* mutant

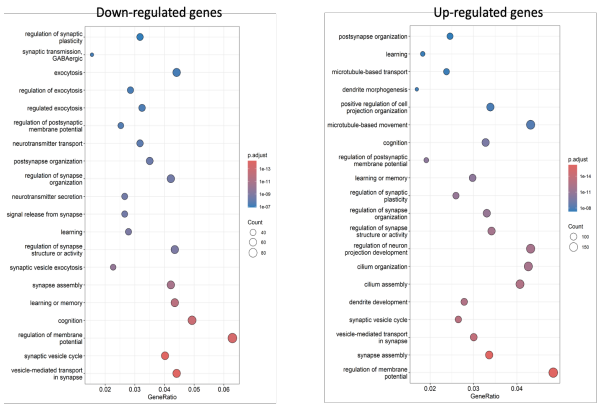

Figure 7: Enriched Gene Ontology (GO) terms for differentially expressed genes in (**A**) astrocytes, (**B**) inhibitory neurons, and (**C**) excitatory neurons from wild-type versus heterozygous or homozygous SYT4-mutant iPSC-derived neurons and heterozygous versus homozygous mutants. Bubble plots show GO terms for down-regulated (left) and up-regulated (right) genes; the x-axis indicates gene ratio, the y-axis lists GO terms, dot size reflects gene count, and dot color represents the level of adjusted P-value.

5.5 Pathway activity analysis using single-cell gene set variation analysis (GSVA)

Hallmark gene-set enrichment analysis revealed distinct pathway alterations in astrocytes associated with *SYT4* genotype. In the astrocyte-specific heatmap (left panel), homozygous *SYT4* mutant astrocytes showed relative enrichment of pathways linked to inflammatory signaling**,** including TNFα/NF-κB, IL6–JAK–STAT3, and interferon responses, as well as pathways associated with fatty-acid metabolism (**Figure 8A, left panel, highlighted in the red rectangle**) In the condition dependent heatmap (**Figure 8A, right panel**), astrocytes displayed progressive pathway alterations across genotypes. Homozygous *SYT4* mutant astrocytes exhibited the strongest enrichment of stress-response and immune-activation pathways, including oxidative phosphorylation, reactive oxygen species signaling, complement activation, and IL6–JAK–STAT3 signaling. Wild-type and heterozygous *SYT4* mutant astrocytes displayed an intermediate profile, with partial attenuation of these pathways. We suggested that this pattern may shift toward a more reactive or stress-adapted astrocyte state under complete *SYT4* deficiency. Violin plots also highlighted the highest level of interferon gamma response and TNF-alpha signaling pathway via NF-KB in homozygous SYT4 mutant condition (**Figure 8B**). Together, these findings indicate that *SYT4* deficiency influences astrocytic inflammatory signaling, and stress-response programs, with homozygous induced the high level of these pathways when comparing with wild type and heterozygous *SYT4* mutant.

WikiPathways enrichment analysis revealed distinct pathway perturbations across astrocytes and transitioning glutamatergic neurons in relation to *SYT4* genotype (**Figure 8C, left panel, highlighted in the red rectangle**). Astrocytes showed enrichment of pathways associated with post covid neuroinflammation, complement system in neuronal development and plasticity, including phosphodiesterase in neuron function. Transitioning glutamatergic neurons showed enrichment of pathways linked to neurotransmitter disorder suggesting altered in neuron development (**Figure 8C, left panel, highlighted in the red rectangle**). In the genotype-stratified heatmap (right panel), we highlighted pathway, which suggested that the post covid neuroinflammation pathway was increased in heterozygous and homozygous *SYT4* mutant condition. Interestingly, the neurotransmitter disorder was strongly expressed in homozygous *SYT4* mutant condition. Collectively, these findings indicate that *SYT4* deficiency enhances inflammation-related pathways in astrocytes, and that homozygous *SYT4* mutants exhibit markedly elevated expression of neurotransmitter-disorder–associated pathways in transitioning glutamatergic neurons. These observations suggested that the most detrimental molecular alterations occur under complete loss of *SYT4* function.

Specific analysis of the WikiPathways “Involvement of Secretases in Neurodegenerative Diseases” gene set revealed differential expression across neuronal lineages (**Figure 8D**, **left panel**). Transitioning glutamatergic excitatory neurons and mature glutamatergic excitatory neurons showed the marked genotype-dependent differences, with heterozygous *SYT4* mutants exhibiting higher expression of secretase-related genes compared with wild type and homozygous *SYT4* mutant (**Figure 8D**, **left panel**). This alteration suggested that excitatory neurons undergoing differentiation, or those already committed to a mature glutamatergic identity, are particularly sensitive to *SYT4* variants in pathways related to neurodegeneration-associated proteostasis.

For the SysNDD intellectual disability related gene module (https://sysndd.dbmr.unibe.ch/) (**Figure 8D**, **right panel**), the alterations were observed in inhibitory neurons, transitioning inhibitory neurons and transitioning glutamatergic excitatory neurons **(Figure 8D**, **right panel and highlighted in red rectangle**). In these populations, heterozygous *SYT4* mutants displayed high expression levels relative to wild type and homozygous *SYT4* mutant, indicating disruption of gene networks associated with synaptic development and cognitive function. Collectively, these findings highlighted that *SYT4* partially mutant also affects neurodegeneration-associated secretase pathways and intellectual disability related gene networks, with the strongest effects observed in some neuronal populations undergoing active synaptic specification and maturation.

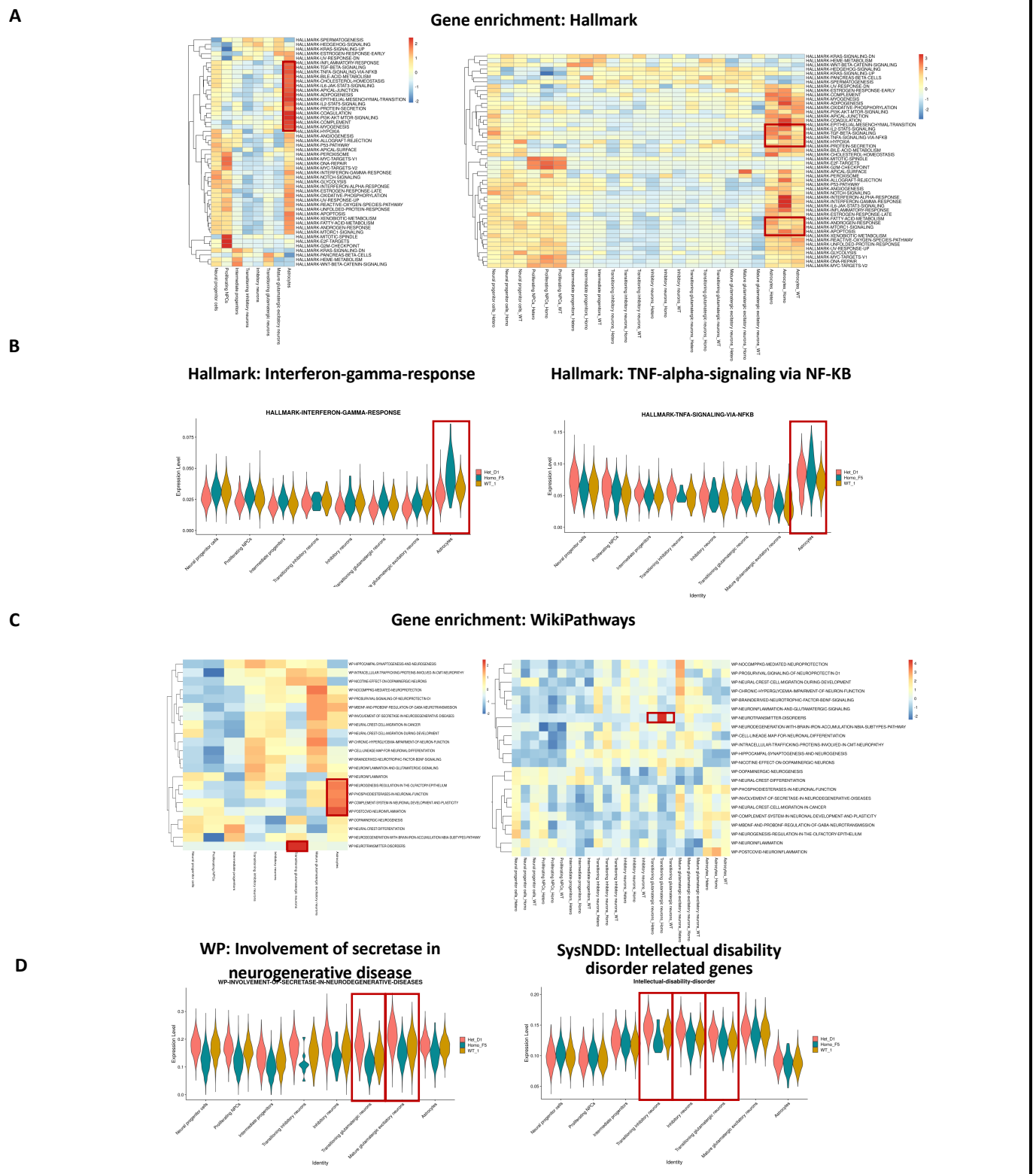

Figure 8: Pathway activity analysis using GSVA. Single-cell gene set variation analysis (GSVA) was used to calculate pathway activity scores for each cell based on its transcriptomic profile. Pathway scores were derived from Hallmark and Wikipathway gene sets in the Molecular Signatures Database (MSigDB). (**A**) Heatmaps showing Hallmark pathway activity across major cell clusters (left) and across experimental conditions within each cell type (right). (**B**) Violin plots depicting the distribution of GSVA scores for the Hallmark “Interferon-gamma response” and “TNF-alpha signaling via NF-κB” pathways across cell types and genotypes. (**C**) Heatmaps showing Wikipathway activity across the same clusters and conditions. (**D**) Violin plots showing GSVA scores for the “WikiPathways: Involvement of secretase in neurodegenerative disease” and “SysNDD: Intellectual disability disorder-related genes” across cell types and genotypes

6. Summary:

For the result of first year, across genome-edited iPSC-derived neuronal cell, *SYT4* variants produced genotype-dependent effects on neuronal differentiation, cellular composition, and molecular pathway activity. scRNA-seq revealed nine major neural and glial populations across all genotypes, although inhibitory neurons and astrocytes were markedly depleted in homozygous mutants, and intermediate progenitors were reduced in heterozygous mutants, suggesting disrupted lineage specification. Trajectory analysis showed that *SYT4* mutation did not disrupt the ability of iPSCs to generate major neural lineages, but it altered lineage composition, which reduced intermediate progenitor cells in the heterozygous *SYT4* mutant, including marked loss of inhibitory neurons and astrocytes in the homozygous *SYT4* mutant. Pseudotime analysis demonstrated a dose-dependent disruption of neuronal differentiation**,** with heterozygous condition expression premature and dysregulated developmental progression, whereas homozygous condition accumulated in immature neuronal states and exhibited impaired terminal maturation. GO enrichment analysis demonstrated that both astrocytes and inhibitory neurons from heterozygous *SYT4* mutants down-regulated neurodevelopmental and synaptic-support pathways while up-regulating cell-cycle, ECM-remodeling, and morphogenesis programs, whereas excitatory neurons exhibited an incomplete compensatory response characterized by impaired synaptic pathways and suppressed translational and mitochondrial gene programs, especially in the homozygous condition. GSVA and WikiPathways analyses further showed pronounced activation of inflammatory and stress-response pathways, such as TNFα/NF-κB, interferon signaling, post-COVID neuroinflammation, and complement-mediated pathways, in astrocytes, alongside strong up-regulation of neurotransmitter-disorder signatures in transitioning glutamatergic neurons under complete *SYT4* loss. Taken together, these findings indicate that *SYT4* deficiency disrupts neuronal maturation and metabolic homeostasis while inducing maladaptive inflammatory and neurodegeneration-associated pathway activation, with homozygous mutants exhibiting the most severe molecular abnormalities.

In the second year of FY2026 joint research grant, we will analyze a second independent set of wild-type and mutant iPSC-derived neuronal clones by scRNA-seq to verify that the observed effects are attributable to the *SYT4* variant rather than clone-specific artifacts. In parallel, we will compare the cellular proteomes of wild-type and mutant iPSC-derived neurons in both clone sets to investigate the correspondence between transcriptomic and proteomic changes. In addition, we will perform functional assays including the identification of SYT4 protein localization, oxidative stress, inflammatory response, calcium imaging, electrophysiology, and synaptic function assays of both the wild type and mutant iPSC-derived neurons. A comprehensive understanding of the molecular mechanisms of SYT4 associated with NS-GDD/ID could potentially lead to the development of novel prognostic and diagnostic markers, and therapeutic strategies for NS-GDD/ID.

7. Future plan: proposed methodology (For Year 2: FY2026 joint research grant)

7.1 Single-cell transcriptomic analysis in set 2 of iPSCs-derived neural cells

The initial processing of raw sc-RNAseq data (FASTQ files) will be conducted using the Cell Ranger pipeline (10x Genomics, version 6.1.2), following a slightly modified version of the methodology described in our previous work [Arora, J et al, *iScience* **2022**]. This involved mapping the sequences to the GRCh38 human reference genome and filtering to retain only cell-associated 10x barcodes. The SoupX package (version 1.6.2) will be employed to eliminate ambient RNA contamination exclusively from the 2D droplet-based scRNA-seq datasets. Subsequent processing of gene expression matrices will be carried out using the Seurat R package (http://satijalab.org/seurat/, version 5.3.1). Seurat objects will be created for each data point and doublets will be identified and excluded using DoubletFinder (version 2.0.3). Cells will be kept for further downstream analyses if the number of detected genes in each cell was between 200 - 3,000 genes per cell, to exclude false and doublet cells. Cells with more than 5% mitochondrial genes will be also removed. An exception will be made for all dataset, where the maximum gene threshold will be adjusted to 6,000 genes per cell due to depth of sequencing. For the iPSC-derived neural cell analysis, the top 2000 variable genes from both samples will be chosen as anchor genes for integration using reciprocal PCA. Clusters will be identified using the Louvain method with the top 30 principal components. Cell types will be identified using a set of established marker genes from the literature.

7.2 In-solution tryptic digestion by filter-aided sample preparation (FASP) method

Equal amount of cellular protein derived from each sample will be pooled and digested by trypsin according to FASP protocol [Singhto, N et al, *J Proteomics* **2018**]. Briefly, the protein mixture in SDT buffer containing 4% SDS, 0.1 M DTT and 100 mM Tris-HCl will be reduced by heating at 95 °C for 5 min. After cooling down at RT, the sample will be transferred to an Omega Nanosep 10 K device (Pall Corporation;), added with 200 µl of 8 M urea in 100 mM Tris-HCl (pH 8.5), and then centrifuged at 14,000 × *g* and RT for 15 min. The recovered proteins will be then alkylated with 100 µl of 50 mM iodoacetamide in 8 M urea/100 mM Tris-HCl (pH 8.5) at 25 °C in the dark using a ThermoMixer® C for 20 min. Thereafter, buffer exchange will be performed twice by centrifugation at 14,000 *g* and 25 °C for 15 min each using 200 µl of 8 M urea/100 mM Tris-HCl (pH 8.5). The proteins will be then finally exchanged into 50 m NH_4HCO_3 and then digested with sequencing grade modified trypsin (Promega; Madison, WI) in 50 mM NH_4HCO_3 at a ratio of trypsin/protein at 37 °C for 16 h. The digested peptides will be collected by transferring the filter unit to a new collection tube and centrifuged at 14,000 × *g* at 25 °C for 15 min. Trypsin activity will be then stopped by adding 10 µl of 5% formic acid in 80% acetronitrile (ACN), and the digested peptides will be dried by a vacuum concentrator (ScanVac;

Lynge, Denmark). The peptides will be finally resuspended in 0.1% formic acid prior to LC-MS/MS.

7.3 iPSCs derived neural cellular proteome identification using SWATH-proteomics

A targeted label-free comparative proteomic analysis will be conducted using Sequential Window Acquisition of all THeorical fragment ions (SWATH)/Data Independent Acquisition (DIA) method as described in our previous studies [Chutipongtanate, S et al, *Sci Rep* **2018**]. Briefly, a total 50 µg proteins will be submitted to an Eksigent nanoLC ultra nanoflow high-performance liquid chromatography coupled with a TripleTOF 6600+ mass spectrometer (ABSciex, Toronto, Canada) run in information-dependent acquisition (IDA) and data-independent acquisition (DIA) modes.

For IDA, mass spectrometry will be operated in positive ion mode for 3500 cycles over 105-min gradient elution, where each cycle performed 1 time of flight (TOF) scan (250 ms accumulation time, 350–1250 *m/z*, 2+ charge state) to acquire the most 100 intense ions. The MS/MS scan will be operated in a high-sensitivity mode (50 ms accumulation time, 50 ppm mass tolerance, 12 s exclusion). For DIA, mass spectrometry will be performed in a range of 350–1500 *m/z* using a predefined mass window of 7 *m/z* with an overlap of 1 *m/z* for 157 transmissible windows. MS scan will be set at 2044 cycles, 1 TOF-MS scan type (50 ms accumulation time over 100–1500 precursor mass range) per cycle with a total cycle time of 3.08 s. The resolutions will be set at 35,000 and 30,000 for the MS1 and SWATH-MS2 scans, respectively, with a collision energy of 15 eV. Raw IDA and DIA data (.tiff) were recorded by Analyst-TF v.1.8 software (ABSciex).

A spectral library will be generated upon 9 IDA experiments (three groups; 3 biological replicates per group) using Protein Pilot v.5.0.2.0 software (ABSciex) against the Swiss-Prot database (UniProtKB 2024_06) *Homo sapiens* (20,421 proteins in the database) with the searching parameters as follows: alkylation on cysteine by iodoacetamide, trypsin enzymatic digestion, 1 missed cleavage allowed, monoisotopic mass, and 1 % false discovery rate (FDR). The group file will be loaded into SWATH Acquisition MicroApp v.2.0.1.2133 in PeakView software v.2.2 (Sciex) to generate the spectral library. The maximum number of proteins will be set as those identified at 1 % global FDR from fit. RT alignment will be performed by the high abundance of endogenous peptides covered in the chromatographic range. SWATH data extraction will be performed using the following parameters: 10-min extraction window, 25 peptides/protein, 6 transitions/peptide, excluding shared peptides, peptide confidence > 99 %, FDR < 1 %, and XIC width of 20 ppm. SWATH extraction data, including the identities and quantities of peptides and proteins, will be exported into an Excel file for further analysis.

7.4 Protein quantification and pre-processing

Label-free quantitative proteomics will be performed on iPSC-derived neurons from wild-type (WT) and *SYT4*-mutant lines. Protein identification and quantification will be carried out using a standard LC–MS/MS workflow, and peptide spectra will be searched against the human Swiss-Prot database (UniProtKB 2024_06). Protein-level intensity values will be exported for downstream analysis in R. Data analysis will be performed in R using the packages limma**,** edgeR**,** dplyr**,** and ggplot2. Proteins annotated as potential contaminants, reverse sequences, or identified by site only will be removed. Intensities with log2-transformed, and proteins detected in fewer than 50% of samples in at least one genotype group (WT or *SYT4* mutant) will be excluded.

7.5 Differential protein expression (DEP) analysis and gene ontology enrichment analysis

Differential protein expression between WT and *SYT4*-mutant neurons in both sets will be assessed using the limma package. A design matrix will be constructed with genotype as the main factor (WT vs *SYT4*-mutant neurons). The lmFit and eBayes functions will be used to fit linear models and compute moderated t-statistics. P-values will be adjusted for multiple testing using the Benjamini–Hochberg method. Proteins with adjusted P-value (FDR) < 0.05 and $|\log_2 \text{ fold change}| \geq 0.58$ (~1.5-fold) will be considered significantly differentially expressed. Gene Ontology (GO) enrichment analysis for Biological Process (BP), Molecular Functions (MF), and Cellular Components (CC) terms will be performed using clusterProfiler with org.Hs.eg.db as the annotation database. Uniprot IDs or protein names were mapped to gene symbols and Entrez IDs using bitr. Up-regulated and down-regulated protein lists will be analyzed separately using enrichGO with pAdjustMethod = "BH", pvalueCutoff = 0.05, and qvalueCutoff = 0.05. Redundant GO terms will be reduced using simplify. Enrichment results will be visualized as dot plots using enrichplot and ggplot2**.**

8. References

1. AlMutiri, R.; Malta, M.; Shevell, M.I.; Srour, M. Evaluation of Individuals with Non-Syndromic Global Developmental Delay and Intellectual Disability. *Children (Basel)* **2023**, *10*, doi:10.3390/children10030414.
2. Banerjee, S.; Munshi, A.; Li, C.; Ayub, M. Editorial: Developmental delay and intellectual disability. *Front Genet* **2022**, *13*, 934815, doi:10.3389/fgene.2022.934815.
3. Aldosari, A.N.; Aldosari, T.S. Comprehensive evaluation of the child with global developmental delays or intellectual disability. *Clin Exp Pediatr* **2024**, *67*, 435-446, doi:10.3345/cep.2023.01697.

4 Singhto, N.; Thongboonkerd, V. Exosomes derived from calcium oxalate-exposed macrophages enhance IL-8 production from renal cells, neutrophil migration and crystal invasion through extracellular matrix. *J Proteomics* **2018**, *185*, 64-76, doi:10.1016/j.jprot.2018.06.015.

5. Chutipongtanate, S.; Greis, K.D. Multiplex Biomarker Screening Assay for Urinary Extracellular Vesicles Study: A Targeted Label-Free Proteomic Approach. *Sci Rep* **2018**, *8*, 15039, doi:10.1038/s41598-018-33280-7.
6. Arora, J.K.; Opasawatchai, A.; Poonpanichakul, T.; Jiravejchakul, N.; Sungnak, W.; Thailand, D.; Matangkasombut, O.; Teichmann, S.A.; Matangkasombut, P.; Charoensawan, V. Single-cell temporal analysis of natural dengue infection reveals

skin-homing lymphocyte expansion one day before defervescence. *iScience* **2022**, *25*, 104034, doi:10.1016/j.isci.2022.104034.
7. Stuart, T.; Butler, A.; Hoffman, P.; Hafemeister, C.; Papalexi, E.; Mauck, W.M., 3rd; Hao, Y.; Stoeckius, M.; Smibert, P.; Satija, R. Comprehensive Integration of Single-Cell Data. *Cell* **2019**, *177*, 1888-1902 e1821, doi:10.1016/j.cell.2019.05.031.3